ADVANCED ENERGY MATERIALS
www.advenergymat.de

Materials Views
www.MaterialsViews.com

A New Model Describing Solid Oxide Fuel Cell Cathode Kinetics: Model Thin Film $SrTi_{1-x}Fe_xO_{3-\delta}$ Mixed Conducting Oxides–a Case Study

WooChul Jung and Harry L. Tuller*

Identifying the important factors governing the oxygen reduction kinetics at solid oxide fuel cell cathodes is critical for enhanced performance, particularly at reduced temperatures. In this work, a model mixed conducting perovskite materials system, $SrTi_{1-x}Fe_xO_{3-\delta}$, is selected, offering the ability to systematically control both the levels of ionic and electronic conductivity as well as the energy band structure. This, in combination with considerably simplified electrode geometry, serves to demonstrate that the rate of oxygen exchange at the surface of $SrTi_{1-x}Fe_xO_{3-\delta}$ is only weakly correlated with either high electronic or ionic conductivity, in apparent contradiction with common expectations. Based on the correlation found between the position of the Fermi energy relative to the conduction band edge and the activation energy exhibited by the exchange rate constant, it is possible to confirm experimentally, *for the first time*, the key role that the minority electronic species play in determining the overall reaction kinetics. These observations lead to a new conceptual model describing cathode kinetics and provide guidelines for identifying cathodes with improved performance.

1. Introduction

Concerns about the environmental consequences of fossil fuel combustion have stimulated interest in developing alternative environment-friendly energy sources. Amongst the various means for achieving improved energy conversion efficiency, the solid oxide fuel cell (SOFC) has received much attention given its high potential conversion efficiency, the flexibility that it offers with respect to fuel choices (hydrocarbons as well as hydrogen) and the reduced emissions associated with electrochemical energy conversion devices.[1]

A key factor hindering SOFC development is the limited degree of understanding regarding the kinetics of the cathode processes and the resultant inability to reduce cathode polarization resistances.[2–6] This is all the more the case when it comes to intermediate temperature SOFC (IT-SOFC) or micro-fabricated SOFC (μSOFC) operating at reduced temperatures (<600 °C), where the cathode polarization resistance become the greatest obstacle to achieving acceptable electrochemical performance.[7–9]

The overall cathode reaction represents the reduction of oxygen from the gas phase and the subsequent transfer of the reduced species into the solid electrolyte (Equation 1). On a more elementary level, however, this reaction is complex and comprises a number of steps (see **Figure 1**a),

$$\frac{1}{2}O_2(gas) + 2e' \rightarrow O_i^{2-} \; O^{2-} + V_O^{\bullet\bullet} \rightarrow O_O^{\times} \qquad (1)$$

including charge transfer steps as illustrated in Figure 1b and discussed in some detail within this article.

During the past decade, cathode performance has seen significant improvement by use of mixed ionic electronic conductors (MIEC) exhibiting simultaneous oxygen ion and electron conduction. The introduction of ionic transport extends the active region for oxygen reduction from the electrolyte/electrode/gas phase triple phase boundary to the full electrode area,[2] providing a superior overall electrode reaction rate. Driven by such improvements, many studies have focused on increasing the ionic transport properties in order to enhance the electrode performance.[9–12] However, for these MIEC electrodes, in nearly all cases, the activation energy for oxygen surface exchange is known to be considerably higher than that for oxygen diffusion.[9,11,13] Accordingly, when operating at reduced temperature, their performance has been largely governed by the kinetics of oxygen exchange at the cathode surface.[2,14] While there have been numerous research efforts directed towards understanding the surface oxygen exchange mechanisms, they remain unsatisfactory and their conclusions controversial.[15–18]

In this work, a new perovskite materials system is selected, offering the ability to systematically control both the levels of ionic and electronic conductivity as well as the energy band structure (see Supporting Information I). This, in combination with considerably simplified electrode geometry, is demonstrated to provide significantly improved insight into the SOFC cathode processes. For this purpose, dense thin film $SrTi_{1-x}Fe_xO_{3-\delta}$ (STF) cathodes, with compositions x = 0.05 to 1.0, were prepared by pulsed laser deposition (PLD), and their

Dr. W. Jung, Prof. H. L. Tuller
Department of Materials Science and Engineering
Massachusetts Institute of Technology
Cambridge, MA 02139, USA
E-mail: wcjung@mit.edu
[+] Current address: Materials Science, California Institute of Technology, Pasadena, CA 91125 USA

DOI: 10.1002/aenm.201100164

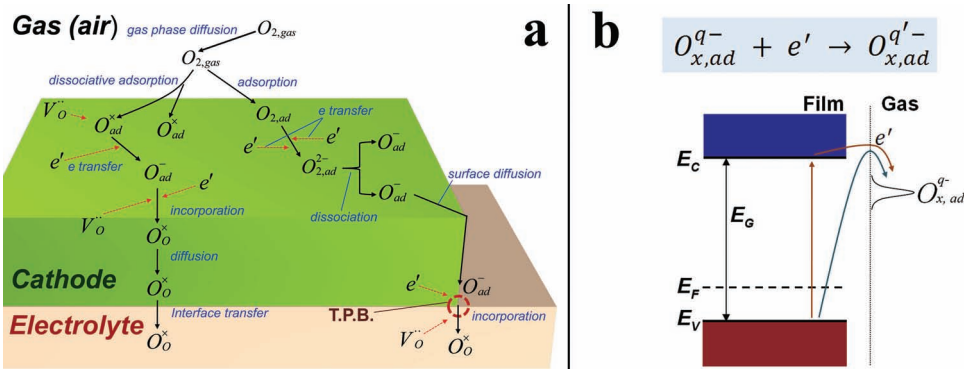

Figure 1. (a) Schematic illustration of possible elementary reaction steps during the cathode reaction. These steps may involve gas phase diffusion, adsorption, electronation, dissociation, diffusion, and finally incorporation of oxygen into the crystal lattice of the electrolyte. For an electronic conductor, the adsorbed oxygen species can be incorporated into the oxide lattice only at the triple phase boundary (TPB), where electrode, electrolyte and gas phase are in contact, while they can penetrate into the MIEC cathode at any point along the surface. (b) Schematic illustration of the electronic band structure and the energy state of the oxygen intermediate ($O_{x,ad}^{q-}$) adsorbed at the surface. Two different possible electron charge transfer pathways are displayed.

cathode reaction kinetics examined as a function of electrode geometry, temperature, oxygen partial pressure and deposition conditions by means of electrochemical impedance spectroscopy (EIS).

Previously, the authors demonstrated that a number of STF compositions, when operated as a cathode, exhibit typical mixed ionic-electronic behavior with the electrode reaction occurring over the full electrode surface area rather than being limited to the triple phase boundary. By systematically varying electrode geometries (e.g., diameter and thickness) and inserting a $Ce_{0.9}Gd_{0.1}O_{2-\delta}$ (CGO) interlayer, the surface oxygen exchange reaction was clearly confirmed to be the rate limiting process as is generally the case for mixed ionic-electronic conductors.[19,20]

In the present contribution, the surface oxygen exchange kinetics are correlated with ionic and electronic transport properties, electronic band structure of STF electrodes over a wide range of x, and as functions of temperature and oxygen partial pressure. Based on the observed findings, suggestions regarding criteria required for optimum MIEC SOFC cathode performance are proposed in terms of the minority electronic carrier density.

2. Results and Discussion

2.1. Physical Characterization of the thin film STF Electrode

The XRD spectra for $SrTi_{1-x}Fe_xO_{3-\delta}$ (STF) thin films with x ranging from 0.05 to 1.0 grown on YSZ (100) single crystal substrates at 700 °C are shown in **Figure 2**. The XRD results obtained for a film of $SrTi_{0.5}Fe_{0.5}O_{3-\delta}$ and from the powder used to make the target with the same composition are displayed in Figure 2a (red) for comparison. The results indicate the films to be polycrystalline perovskite phase with highly (110) oriented texture over the whole range of Fe fraction. Limited reflections from (100) or (111) are sometimes observed above background noise level (see insert in Figure 2b). There is no evidence of amorphous films, or diffraction peaks other than the ones in the cubic perovskite phase. AFM images were also used to confirm that the electrodes used in this work exhibit well-defined geometries with extremely flat and smooth surfaces (< several nm roughness), compared with typical SOFC electrode morphologies (see Supporting Information II).

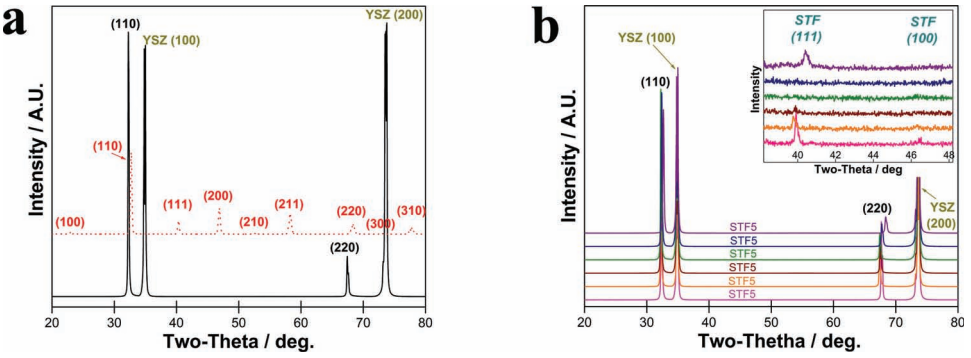

Figure 2. (a) XRD pattern of a 137 nm thick $SrTi_{0.5}Fe_{0.5}O_{3-\delta}$ film deposited on a YSZ single crystal with (100) orientation by pulsed laser deposition at 700 °C. The pattern indicates preferred (110) orientation. XRD results from the powder used to make the target with the same composition are also displayed in red for comparison. (b) XRD patterns of $SrTi_{1-x}Fe_xO_{3-\delta}$ films with ~140 nm thickness on a (100) YSZ single crystal as a function of different Fe composition between 5 and 100 mol%.

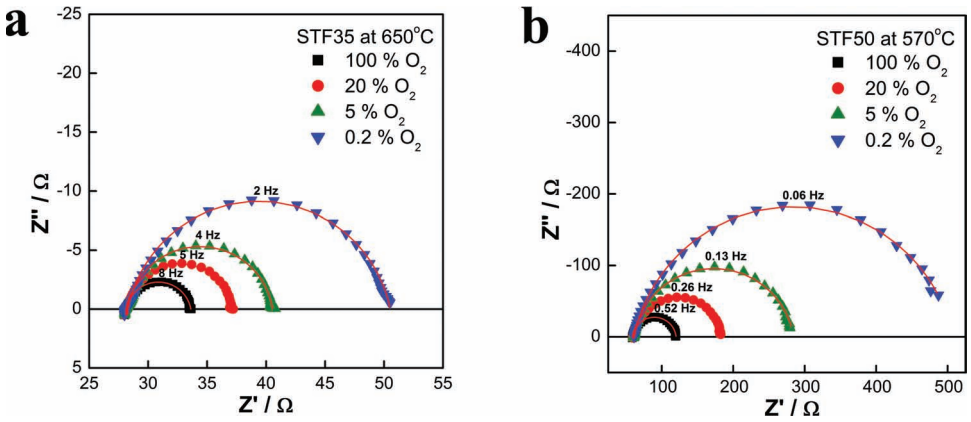

Figure 3. Typical impedance spectroscopy plots of (a) STF35 at T = 650 °C, (b) STF50 at T = 570 °C as a function of pO_2.

2.2. Analysis of Electrochemical Impedance Spectroscopy

A key feature of Impedance spectroscopy is its ability to show features in its spectrum derived from different processes active in the bulk and at interfaces of often complex electrical or electrochemical systems. In this work, the origins of the key resistive contributions to the impedance spectra obtained for STF films on YSZ were systematically analysed by examining the dependence on temperature, pO_2 and device geometry.

A symmetrical structure with identically sized (9 mm x 9 mm) STF thin film electrodes on both sides of the YSZ electrolyte was prepared for EIS measurements. **Figure 3** shows typical EIS results obtained for the symmetrical structure for STF electrodes of composition x = 0.35 and 0.50, designated as STF35 and STF50, respectively. For all Fe compositions, the impedance spectrum exhibits an offset resistance (R_{off}) followed by a nearly ideal semicircle at lower frequency. Several features of the offset resistance (R_{off}) are consistent with the source being the bulk resistance of the YSZ electrolyte single crystal substrate. This includes the activation energy of R_{off} of ~ 0.95 eV and its pO_2 independence. Furthermore, the magnitude of conductivity (0.24×10^{-3} S/cm at 650 °C), calculated based on the present cell electrode geometry, electrolyte thickness and measured R_{off}, agrees well with the literature data for the ionic conductivity of YSZ (e.g. 0.53×10^{-3} S/cm).[21] Lastly, R_{off} was found to be independent of electrode composition. One can thus confidently conclude that this IS feature should be attributed to the YSZ electrolyte.

Accordingly the remaining low frequency spectra is attributed to the STF electrode response,[19] which given its near ideal semicircular shape, can be modeled by a parallel *R*-*C* circuit. More generally, the capacitor is replaced by a constant phase element (CPE), for which the overall impedance is given by

$$Z = \frac{1}{Q(iw)^n} \tag{2}$$

The effective capacitance can be extracted from this expression,[22] by

$$C = Q\omega_{max}^{n-1} = (R^{1-n}Q)^{1/n} \tag{3}$$

which corresponds, for example, to a *C* value of approximately 12 mF/cm^2 for a 160 nm thick STF50 film at 650 °C (typical n value between 0.92 and 0.99). This exceptionally high *chemical* capacitance is typical of mixed conducting electrodes.

Previously the *R* values derived from this part of the EIS spectra were examined by geometrical dependence on film thickness and electrode radius and insertion of a CGO interlayer, concluding that the limiting process in this work must be attributed to the surface oxygen exchange reaction occurring at the surface of the STF electrodes.[19,20] For a detailed discussion of how the how the impedance spectra of these thin film structures were analyzed, the reader is referred to Supporting Information III. In the following, the *R* values derived from this part of the EIS spectra will be discussed, focusing on the electrode kinetics.

2.3. Surface Oxygen Exchange Kinetics of STF Electrode

The area-normalized electrode resistance, R_{STF}, obtained by EIS measurements in air, is plotted as a function of reciprocal temperature and oxygen partial pressure in **Figure 4**a and 4b respectively both as a function of the STF Fe fraction. Since the STF electrode resistance is governed by the surface oxygen exchange reaction, R_{STF} is an indicator of how slow or fast oxygen surface exchange takes place on the STF electrodes. Since the surface area can be precisely determined for thin films, the corresponding kinetic parameter, *k* (surface oxygen exchange coefficient), may be extracted from the measured electrode resistance, according to equation 4,[23] as;

$$k = \frac{k_B T}{4e^2 R_S c_o} \tag{4}$$

(k_B: Boltzmann constant, *e*: electron charge, *T*: temperature, R_s: area specific resistance and c_o: total concentration of lattice oxygen with the value 4.92×10^{22} cm^{-3} used in this calculation).[24] Calculated *k* values, averaged over values obtained from three or more different samples are shown in **Table 1**.

While there is a reduction in R_{STF} (or increase in *k*) with increasing Fe, the rate of change decreases so that R_{STF} reaches near saturation above x = 0.35 (STF35). For comparison, the *R* values for dense thin films of the more typical MIEC cathodes

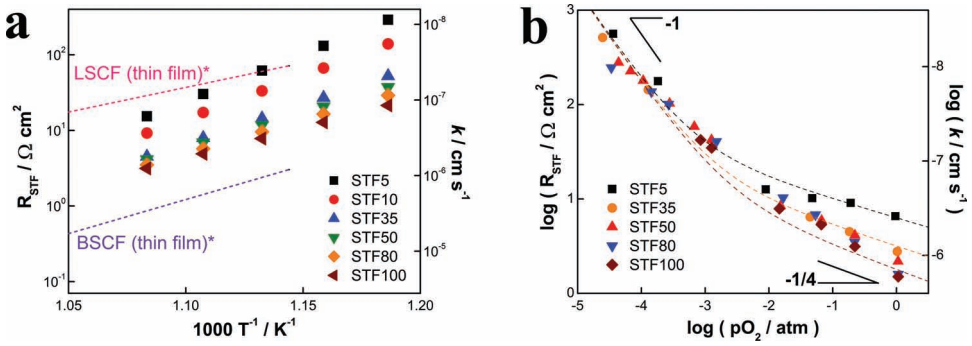

Figure 4. (a) Temperature dependence of R_{STF} for STF electrodes in this work (solid symbols), and other dense thin film MIEC electrodes (LSCF and BSCF) fabricated by PLD (dashed lines). The data for the STF electrodes and for the other MIEC electrodes were obtained respectively from the authors' earlier work,[20] and the work of Baumann, et al.[13] (b) Double-logarithmic plots of the area specific resistance for STF electrodes vs pO_2 measured at 650 °C. Note: the local pO_2 of the electrode will also depend on the overpotential on the electrode and that the data in these figures could be used to predict properties for polarized electrodes.

prepared by PLD are also inserted in Figure 4a. The area specific resistance values of the thin film STF electrodes are found to be comparable in magnitude to those of thin film $La_{0.6}Sr_{0.4}Co_{0.2}Fe_{0.8}O_3$ (LSCF), the most commonly used MIEC cathode material at intermediate temperatures,[8,25–27] pointing to the suitability of STF as a realistic model mixed conducting cathode material. What is surprising, however, is that this is true even though the electronic conductivity (σ_{el}) of the STF cathodes is as much as a factor of ~165,000 lower than that of LSCF (σ_{el} = 330 S/cm,[28] at 650 °C, k^* = 6 ×10^{-7} cm/s,[29] at 663 °C). It would appear that a σ_{el} as low as 2 × 10^{-3} (S/cm) (650 °C for STF5) is sufficient to obtain reasonably high surface exchange kinetics (k = 1.65 ×10^{-7} cm/s at 650 °C).

2.4. Correlation Between Oxygen Exchange Kinetics and Materials Properties

2.4.1. k vs. Transport Properties

From a fundamental point of view, exchange reactions differ from bulk transport reactions in that the former reflects a transfer reaction across an interface between two different phases, i.e., a solid/ gas interface, while the latter takes place in a homogeneous medium. Nevertheless, the important role that bulk transport kinetics play in achieving fast oxygen exchange reactions at oxide surfaces has often been reported.

Table 1. Activation energies and surface oxygen exchange coefficients for STF samples with different Fe mol%. E_a was obtained from impedance measurements in the temperature range 570–650 °C in air. k was calculated from the R_{STF} results at 650 °C in air.

Fe mol%	E_a/ eV	k/ cms^{-1}
5	2.47 ± 0.08	1.65 × 10^{-7}
10	2.28 ± 0.18	2.74 × 10^{-7}
35	2.06 ± 0.13	5.61 × 10^{-7}
50	1.84 ± 0.10	6.11 × 10^{-7}
80	1.77 ± 0.09	7.21 × 10^{-7}
100	1.61 ± 0.07	8.05 × 10^{-7}

Boukamp, et al. were the first to note that oxides with high σ_{el} exhibit superior surface exchange coefficients.[30] Much has also been made of the surprising empirical correlations between k^* and D^* found by Kilner and co-workers after reviewing a large number of tracer oxygen exchange data sets obtained from various acceptor-doped fluorites and perovskites.[31] The existence of such a correlation has been interpreted by Merkle and co-workers as an indication that oxygen vacancies often play the dominant role in the surface exchange process.[32] De Souza recently developed an empirical, atomistic expression based on the same correlation, suggesting that the availability of electronic species determines the rate of oxygen exchange.[33] In general, it is an accepted rule of thumb that either high electronic or ionic conductivities or both are necessary for obtaining fast oxygen exchange reactions. Nevertheless, to the authors' best knowledge, the fundamental reasons for this correlation may still be regarded as an open question.

To understand the relative role of the bulk transport properties in influencing electrode surface oxygen exchange kinetics, both σ_{el} and σ_{ion} values from bulk STF samples with different Fe compositions are examined and plotted together with respective k values in **Figure 5**, σ_{el} and σ_{ion} change by nearly five and four orders of magnitudes, respectively, in going from STF with 5 to 100 mol% Fe, while k remains largely within the same

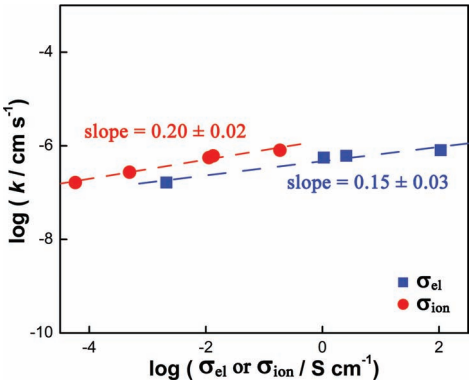

Figure 5. Double-logarithmic plot between the surface exchange coefficient (k), and the electronic and ionic conductivities (σ_{el} and σ_{ion} for bulk STF) obtained for various Fe compositions at 650 °C air.

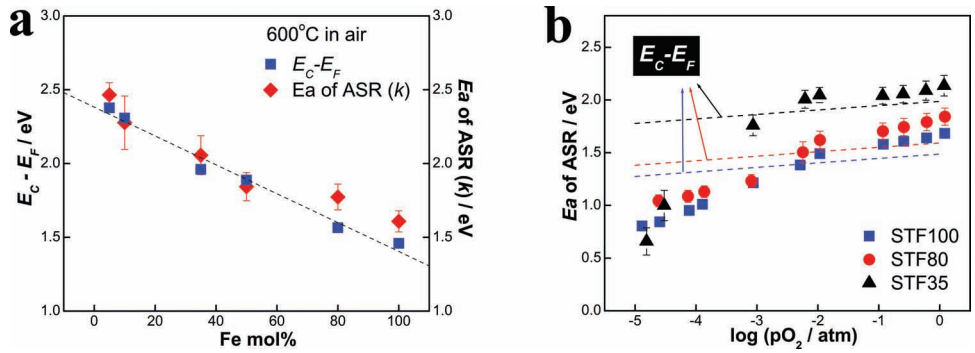

Figure 6. (a) Calculated E_C-E_F (left axis) and activation energy of R_{STF} (or k) measured by EIS (right axis) as a function of Fe composition at 600 °C in air. (b) Activation energy of R_{STF} (or k) as a function of pO_2 at 600 °C for STF35, 80, and 100. The corresponding E_C-E_F values (dashed lines) are also included for comparison.

order of magnitude. Here one finds a weak dependence of k on both σ_{el} and σ_{ion} with a power law dependence of 0.15 ± 0.03 and 0.20 ± 0.02, respectively (see Figure 5). This suggests that oxygen exchange is only weakly correlated with the transport properties of the majority electronic and ionic species. Furthermore, the activation energy, characteristic of k, has always been found to be much greater than those of σ_{el} and σ_{ion}, e.g., for thin film STF50: E_a (k) = 1.84 eV vs $E_a(\sigma_{el})$ = 0.17 eV and $E_a(\sigma_{ion})$ = 0.66 eV, the latter obtained for bulk STF50. Therefore, it is reasonable to conclude that the electrical conductivity, at least above a certain minimum value, does not play the limiting role in surface exchange reactions.

2.4.2. k vs. Electronic Band Structure

Surface oxygen exchange requires several electron transfer processes in series to reduce the oxygen molecule to a doubly charged oxygen ion capable of being inserted into the oxide lattice. Since the combination of both high electronic and ionic transport does not seem to be a critical factor for the exchange kinetics, one may alternatively consider charge transfer as the possible RDS. Determining the efficiency of electron transfer from the catalyst surface to the reactant molecules has been an important topic in the study of catalysts as well as surface science for decades.[34–37] More generally, the electronic band structure, and the corresponding position of the Fermi level (E_F) with respect to the molecular oxygen level or the conduction band edge at the surface, is considered a key factor in governing the rate of electron transfer (see Figure 1b).

To examine its relative importance in the surface oxygen exchange reaction, the position of E_F relative to the bottom edge of the conduction band (E_C) was determined, based on the thermodynamic parameters defining defect generation in the STF system previously reported by the authors.[24] While recognizing the limitations of applying the reported dilute solution model describing the defect structure of STF to predict the electron density, n (T, pO_2, Fe) for a wide range of x, it nevertheless provides an accurate predictive description of the observed experimental transport and stoichiometry data. It is, therefore, tempting to utilize this model to calculate the position of the Fermi level in STF relative to the conduction band edge as a function of temperature, pO_2 and Fe content and examine how its position might be correlated with the surface exchange kinetics. Furthermore, even for high Fe concentrations, for which hole concentrations in these p-type materials reach high concentrations, i.e., E_F lies within 3kT of the valence band edge, we assume that non-degenerate semiconductor statistics apply when correlating the position of E_F relative to the bottom edge of the conduction band (E_C) (E_C-E_F>1.5 eV) and the electron density, n. Under those conditions, E_C-E_F is given by

$$E_C - E_F = -kT \ln\left(\frac{n}{N_C}\right) \quad (5)$$

where N_C is the effective density of states in the conduction band and n is the electron density.[38] **Figure 6**a shows E_C-E_F, calculated in this way at 600 °C in air, plotted as a function of Fe fraction. E_F is seen to move toward the conduction band edge with increasing Fe, largely resulting from the reduction in the band gap of the STF system,[24] (see Supporting Information I). As expected from its p-type conducting nature, E_F lies close to the top of the valence band.

When plotting the activation energy of R_{STF} (or k) for the surface oxygen exchange reaction together with the Fermi level position, one finds a surprisingly good correlation between the two. As shown in Figure 6a, both quantities, not only share a decreasing trend with increasing Fe composition, but also agree well with respect to their absolute magnitudes. While the Fermi level position relative to the conduction band and the activation energy of k are not normally considered in the same context, the strong correlation observed in this study clearly implies that an electron transfer process must be involved in the RDS for oxygen reduction at the surface of the STF cathode.

A similar correlation was observed by Merkle and coworkers,[39] reporting that the rate of oxygen exchange into lightly (<0.3%) Fe doped $SrTiO_3$ was enhanced by more than a hundredfold upon UV illumination. However, they argued that the UV enhancement was only valid for lightly doped systems, and therefore concluded that ionic transport governs the overall oxygen reduction in heavily Fe doped or highly mixed conducting oxide systems.[40] To author's best knowledge, the observations in this work, are the first experimental results demonstrating the importance of the minority electron carrier density in controlling the oxygen exchange reaction in mixed conducting SOFC cathodes.

Further confirmation of the correlation has been achieved by examining their pO_2 dependent behaviors. Figure 6b shows how E_a (k) and E_C-E_F vary as a function of pO_2 at 600 °C. E_F moves toward the conduction band edge upon reduction given that the electron density increases. Again, both the E_a (k) and E_C-E_F show a similar trend, i.e. a nearly linear decrease in value with decreasing log pO_2, in the high pO_2 regime (> 10^{-2} atm). Consequently, focusing on the high pO_2 regime (> 10^{-2} atm), the formation of surface oxygen intermediate species, $O_{x,ad}^{q-}$, by electron transfer is assumed to be the most likely RDS as described in the following.

$$O_{x,ad}^{q-} + e' \rightarrow O_{x,ad}^{(q+1)-1} \text{ (where } x = 1 \text{ or } 2 \text{ and } q = 0 \text{ or } 1) \quad (6)$$

The e' on the left hand side of the equation comes from the conduction band of the STF cathode, which, given the p-type nature of STF, implies an electron/hole generation (band-to-band transition) step prior to the electron transfer across the oxide surface (see Figure 1b). Since the electron density in the conduction band is directly determined by the energy difference between E_C and E_F (see Equation 5), it therefore explains why the activation energy of the surface exchange reaction, E_a (k), parallels the dependence of E_C-E_F on both Fe fraction and pO_2. In fact, the characteristic ¼ slope dependence of log k on log pO_2 (see Figure 4b) is also known to be typical of the charge transfer reaction, as reported for various metal and oxide cathodes.[2,33,41] Furthermore, it also explains why the exchange reaction is not strongly dependent on the ionic transport properties nor on the majority p-type conductivity.

2.4.3. Surface Exchange at Reduced pO_2 (<10^{-3} atm)

A much sharper drop in E_a is observed with decreasing log pO_2 at more reduced atmospheres (<10^{-3} atm) as well as a convergence in the magnitude of E_a for all values of Fe (see Figure 6b). Similarly, the pO_2 dependence of R_{STF}, plotted in Figure 4b, exhibits a rather sharp change at a $pO_2 \sim 10^{-3}$ atm. Accordingly, one may conclude that there are at least two different rate determining steps (RDS) competing with each other under the measurement conditions in this study. This is supported by the fact that R_{STF} at reduced pO_2 (<10^{-3} atm) remains nearly independent of Fe fraction, while it is clearly dependent on Fe fraction at higher pO_2. **Table 2** summarizes the dependences of R_{STF} on pO_2^{-m} (where m defines the power law dependence of log R_{STF} on pO_2), temperature, and Fe composition. Consequently one is motivated to conclude that while electron transfer is the RDS at high pO_2, another process takes over at lower pO_2.

A strong pO_2 sensitivity of k, in general, implies that the RDS involves molecular oxygen (O_2) adsorption processes on the cathode surface.[15,33,39] Accordingly, chemisorption or dissociative adsorption of molecular oxygen is considered to be the possible RDS. In fact, this type of reaction is often assumed to be limited by the availability of surface oxygen vacant sites,[2,15] which increases with increasing Fe in STF. However, it is worth noting that STF exhibits very high levels of oxygen vacancies, [$V_O^{\bullet\bullet}$], even at the lowest Fe level (5 mol%) examined in this work. It would therefore not be surprising to find that the availability of surface oxygen vacancies is more than sufficient to satisfy the adsorption or incorporation reaction; rather the RDS may be limited instead by the availability of adsorbed oxygen species at low pO_2.

A simple calculation has been performed comparing the relative surface coverage of oxygen with the availability of oxygen vacancies. Considering [$V_O^{\bullet\bullet}$] of 1.65×10^{20} cm^{-3} for STF5 at 650 °C, a surface vacancy density of 3.01×10^{13} cm^{-2} is estimated by:

$$([V_o^{\bullet\bullet}])^{2/3} = (1.65 \times 10^{20} cm^{-3})^{2/3} = 3.01 \times 10^{13} cm^{-2} \quad (7)$$

Experimental studies suggest that the surface coverage of oxygen adsorbates on titanium oxides normally does not exceed ~10% of the total available sites at the surface. For charged adsorbates, with Mott–Schottky depletion layers and typical band bending, Weisz predicts a maximum surface coverage of below 1%.[41,42] By assuming a total number of available adsorption sites per unit area of 6.45×10^{14} cm^{-2} (i.e. approx. one adsorption site per perovskite unit cell), one obtains a maximum surface oxygen density of 6.45×10^{13} cm^{-2} (i.e. 10% of the available sites). In fact, this value is consistent with reported saturation oxygen at much reduced temperature (<300 K).[43–45] Given the thermal desorption behavior of the surface adsorbates as well as the fact that no TPD peak was obtained at temperatures higher than 500 K,[45] it is reasonable to assume that the actual surface coverage would be considerably smaller than the maximum estimated value. Accordingly, this indicates the number of available vacant sites is even greater than that of the adsorbed oxygen species at the oxide surface at reduced pO_2 even with the least amount of Fe, 5 mol%.

Table 2. Dependence of R_{STF} on pO_2, temperature, and Fe composition, obtained in the work.

Low pO_2 regime	High pO_2 regime
Strong pO_2 sensitivity of R_{STF} (or k); m = 1	Weaker pO_2 sensitivity of R_{STF} (or k); m = 1/4
Lower activation energy, e.g. ~1 eV	Higher activation energy, e.g. ~2 eV
No dependence on Fe composition	Dependence on Fe composition

2.5. Criteria Required for Optimum MIEC SOFC Cathode Performance

Based on the findings for the surface oxygen exchange reaction in this study, some suggestions for criteria for achieving optimum SOFC MIEC cathode performance can be made.

First, given the fact neither the electronic nor the ionic conductivity in themselves limit the overall exchange reaction kinetics, one can define criteria regarding the minimum required values of σ_{el} and σ_{ion} needed to achieve good cathode performance. In STF, both conductivities increase with increasing Fe. The lowest level of Fe used in this work was 5 mol%, which corresponds to σ_{el} of 2.1×10^{-3} S/cm and σ_{ion} of 5.75×10^{-5} S/cm at 650 °C in air. In fact, typical MIEC cathode materials such as (La,Sr)CoO_3, (La,Sr)(Co,Fe)O_3, and (Ba,Sr)(Co,Fe)O_3 provide much more highly conducting properties, certainly desireable for current collection. However, these parameters, based on the findings of this study, are likely not the critical factors controlling their surface exchange kinetics.

Second, one finds the minority electron in these p-type materials to be the critical specie governing the surface exchange

reaction kinetics. This involves the excitation of electrons to the conduction band with subsequent electron transfer from the oxide surface to the oxygen adsorbate at the surface. This implies the need for a high density of electrons to accelerate the kinetics. Achieving a high electron density in cathode materials, however, is not straightforward given that these materials become highly oxidized during SOFC operation, i.e. under high oxygen partial pressures and temperatures. Typical MIEC cathode materials contain transition metals such as Mn, Fe and Co. It is well known that the readily reduced metals (Fe & Co) provide additional oxygen vacancies leading to enhanced cathode performance. However, the ease of reduction of Fe and Co leads not only to additional oxygen vacancies, but also to extra electrons in the conduction band and thereby a lifting of the position of the Fermi level towards the conduction band edge. This, therefore, points to a further reason for selecting easily reduced transition metals leading to improved cathode performance.

3. Conclusions

While SOFC metal oxide cathodes have been the subject of numerous studies, the mechanisms controlling their behavior have remained poorly understood. This has been due to a number of factors including the morphological complexity of the electrode and the electrode- electrolyte interface, the limited understanding of the defect/transport/energy band structure correlations and the evolution of the surface chemistry with varying operating conditions. In this work, it has been possible, *for the first time,* to provide a direct link between the bulk and surface properties, i.e. between the bulk minority electron density and the cathode electrode impedance or equivalently in this study, the oxygen surface exchange coefficient. The observation that the rate of oxygen exchange for mixed conducting cathode materials in SOFC may be largely determined, not by the fast transport properties of the majority electronic and ionic carriers, but by the availability of minority carriers–electrons in the excited state–should aid in directing future research into the physics of these material as well as providing improved guidelines towards the development of cathodes with improved performance at reduced temperatures.

4. Experimental Section

Sample preparation and characterization: STF thin films were prepared by means of pulsed laser deposition (PLD) from oxide targets of the respective materials and deposited onto (100) oriented single crystal yttria doped zirconia (YSZ) substrates for EIS measurement. One inch diameter oxide targets were prepared by the conventional mixed-oxide technique starting from iron (III) oxide (Alfa Aesar, 99.945%), strontium carbonate (Alfa Aesar, 99.99%), and titanium (IV) oxide (Alfa Aesar, 99.9%) powders. A Coherent (Santa Clara, CA) COMPex Pro 205 KrF eximer laser, emitting at a wavelength of 248 nm, was used for ablation. The deposition parameter configuration was 400 mJ/pulse laser energy, 8 Hz laser repetition rate, and an O_2 working pressure of 10 mTorr. Film thicknesses ranging between 70 and 500 nm were determined by surface profilometry (Tencor P-10). Detailed information regarding oxide target preparation and PLD deposition conditions can be found in previous studies.[19,20]

X-ray diffraction (XRD) measurements were performed on synthesized powders and deposited films using a Bragg-Brentano diffractometer (Rigaku RU300, Tokyo, Japan, Cu Kα wavelength ($\lambda = 1.541$Å)). The grain size, morphology, and surface roughness of the STF thin films were characterized by a Vecco Metrology (Santa Barbara, CA) D3000 atomic force microscope (AFM) with a Nanoscope IIIa controller. Micrographs were analyzed to determine the root mean square (RMS) surface roughness and grain size using Vecco's Nanoscope software (version 5.12r3).

Electrical and electrochemical measurements: A symmetrical structure, with identically sized STF electrodes on both sides of the YSZ electrolyte, was used for EIS measurements. Au mesh and Au paste were placed on each STF electrode surface, serving as current collectors. In order to confirm that any possible interactions between the Au and the oxygen did not influence the impedance spectra, photo-lithographically defined platinum patterns were sometimes fabricated between the YSZ substrate and the STF film, serving as a buried current collector. Both a custom-designed enclosed probe station, manufactured by McAllister Technical Services (Coeur d'Alene, ID) and a tube furnace were used for the EIS measurements at temperatures between 570 °C and 650 °C and between 2×10^{-5} atm to 1 atm. EIS measurements, covering the frequency range from 7 mHz to 1 MHz, with amplitude of 20 mV, were performed with a Solarton 1260 or 1250 impedance analyzer operated in combination with a Solartron 1286 potentiostat/galvanostat.

Supporting Information

Supporting Information is available from the Wiley Online Library or from the author.

Acknowledgements

This work was initially supported by the Ceramics Program, Division of Materials Research Directorate for Mathematical & Physical Sciences, National Science Foundation under award DMR-0243993 and continued under the Materials Science and Engineering Division, Office of Basic Energy Sciences, Department of Energy under award DE SC0002633. W.J. Thanks the Samsung Foundation for fellowship support. The authors thank Dr. R.A. De Souza and Dr. J. Fleig for helpful discussions. The x-ray, XPS and AFM facilities of the Center for Materials Science and Engineering, an NSF MRSEC funded facility were used in this study.

Received: April 4, 2011
Revised: July 21, 2011
Published online: September 8, 2011

[1] N. Q. Minh, *J. Am. Ceram. Soc.* **1993**, *76*, 563.
[2] S. B. Adler, *Chem. Rev.* **2004**, *104*, 4791.
[3] S. M. Haile, *Acta. Mater.* **2003**, *51*, 5981.
[4] A. J. Jacobson, *Chem. Mater.* **2009**, *22*, 660.
[5] R. M. Ormerod, *Chem. Soc. Rev.* **2003**, *32*, 17.
[6] J. Richter, P. Holtappels, T. Graule, T. Nakamura, L. J. Gauckler, *Mon. Chem.* **2009**, *140*, 985.
[7] N. P. Brandon, S. Skinner, B. C. H. Steele, *Ann. Rev. Mater. Res.* **2003**, *33*, 183.
[8] D. J. L. Brett, A. Atkinson, N. P. Brandon, S. J. Skinner, *Chem. Soc. Rev.* **2008**, *37*, 1568.
[9] Z. P. Shao, S. M. Haile, *Nature* **2004**, *431*, 170.
[10] S. Li, Z. Lü, N. Ai, K. Chen, W. Su, *J. Power Sources* **2007**, *165*, 97.
[11] L. Wang, R. Merkle, J. Maier, *J. Electrochem. Soc.* **2010**, *157*, B1802.
[12] C. Xia, W. Rauch, F. Chen, M. Liu, *Solid State Ion.* **2002**, *149*, 11.
[13] F. S. Baumann, J. Fleig, G. Cristiani, B. Stuhlhofer, H. U. Habermeier, J. Maier, *J. Electrochem. Soc.* **2007**, *154*, B931.

[14] J. Fleig, J. Maier, *J. Eur. Ceram. Soc.* **2004**, *24*, 1343.
[15] S. B. Adler, X. Y. Chen, J. R. Wilson, *J. Catal.* **2007**, *245*, 91.
[16] G. W. Coffey, L. R. Pederson, P. C. Rieke, *J. Electrochem. Soc.* **2003**, *150*, A1139.
[17] M. Liu, *J. Electrochem. Soc.* **1998**, *145*, 142.
[18] M. Prestat, J. F. Koenig, L. J. Gauckler, *J. Electroceram.* **2007**, *18*, 87.
[19] W. Jung, H. L. Tuller, *J. Electrochem. Soc.* **2008**, *155*, B1194.
[20] W. Jung, H. L. Tuller, *Solid State Ion.* **2009**, *180*, 843.
[21] P. S. Manning, J. D. Sirman, R. A. De Souza, J. A. Kilner, *Solid State Ion.* **1997**, *100*, 1.
[22] J. Fleig, *Solid State Ion.* **2002**, *150*, 181.
[23] F. S. Baumann, J. Fleig, H. U. Habermeier, J. Maier, *Solid State Ion.* **2006**, *177*, 1071.
[24] A. Rothschild, W. Menesklou, H. L. Tuller, E. Ivers-Tiffée, *Chem. Mater.* **2006**, *18*, 3651.
[25] J.-M. Bae, B. C. H. Steele, *Solid State Ion.* **1998**, *106*, 247.
[26] M. Prestat, J.-F. Koenig, L. J. Gauckler, *J. Electroceram.* **2007**, *18*, 87.
[27] B. C. H. Steele, *J. Power Sources* **1994**, *49*, 1.
[28] L. W. Tai, M. M. Nasrallah, H. U. Anderson, D. M. Sparlin, S. R. Sehlin, *Solid State Ion.* **1995**, *76*, 273.
[29] S. J. Benson, R. J. Chater, J. A. Kilner, in *Proc. of the 3rd Int. Symp. on Ionic and Mixed Conducting Ceramics*, The Electrochemical Society Proceedings Series, Pennington, **1997**.
[30] B. A. Boukamp, H. J. M. Bouwmeester, A. J. Burggraaf, in *Proc. of the 2nd Int. Symp. on Ionic and Mixed Conducting Ceramics.* (Eds: T. A. Ramanarayanan, W. L. Worrell, H. L. Tuller), The Electrochemical Society Proceedings Series, Pennington, **1994**.
[31] R. A. De Souza, J. A. Kilner, *Solid State Ion.* **1999**, *126*, 153.
[32] R. Merkle, J. Maier, H. J. M. Bouwmeester, *Angew. Chem.-Int. Edit.* **2004**, *43*, 5069.
[33] R. A. De Souza, *Phys. Chem. Chem. Phys.* **2006**, *8*, 890.
[34] J. Greeley, J. K. Nørskov, M. Mavrikakis, *Annu. Rev. Phys. Chem.* **2002**, *53*, 319.
[35] B. Hammer, J. K. Nørskov, *Nature* **1995**, *376*, 238.
[36] W.-X. Li, C. Stampfl, M. Scheffler, *Phys. Rev. Lett.* **2003**, *90*, 256102.
[37] J. K. Nørskov, J. Rossmeisl, A. Logadottir, L. Lindqvist, J. R. Kitchin, T. Bligaard, H. J. K. Jonsson, *J. Phys. Chem. B* **2004**, *108*, 17886.
[38] D. A. Neamen, In *Semiconductor Physics and Devices, Basic Principles, 3rd Edition.* (McGraw Hill, New York, NY, **2003**).
[39] R. Merkle, J. Maier, *Phys. Chem. Chem. Phys.* **2002**, *4*, 4140.
[40] R. Merkle, J. Maire, *Angew. Chem.-Int. Edit.* **2008**, *47*, 3874.
[41] J. Fleig, R. Merkle, J. Maier, *Phys. Chem. Chem. Phys.* **2007**, *9*, 2713.
[42] P. B. Weisz, *J. Chem. Phys.* **1953**, *21*, 1531.
[43] J. M. Pan, B. L. Maschhoff, U. Diebold, T. E. Madey, *J. Vac. Sci. Technol. A-Vac. Surf. Films* **1992**, *10*, 2470.
[44] G. Q. Lu, A. Linsebigler, J. T. Yates, *J. Chem. Phys.* **1995**, *102*, 4657.
[45] M. A. Henderson, W. S. Epling, C. L. Perkins, C. H. F. Peden, U. Diebold, *J. Phys. Chem. B* **1999**, *103*, 5328.